Low-Loss Ultrawideband Programmable RF Photonic Phase Filter for Spread Spectrum Pulse Compression

Hyoung-Jun Kim, *Member, IEEE*, Amir Rashidinejad, *Member, IEEE*, and Andrew M. Weiner, *Fellow, IEEE*

***Abstract*—We demonstrate a low-loss, ultrawideband (UWB), programmable radio frequency photonic phase filter utilizing a broadband optical frequency comb, interferometric pulse shaping configuration, and a balanced photodetector for spread spectrum pulse compression. We present UWB linear frequency-chirped pulse compression with bandwidths exceeding 7 GHz. The filter insertion loss for these experiments can be as low as 0.5 dB. In addition, the bandwidth and chirp rate of the phase filter are programmable. To further illustrate the programmability of the proposed filter, we report pulse compression experiments for UWB Costas sequences with bandwidth over 6 GHz. Finally, we perform a spread-spectrum jamming-resistant pulse compression experiment with the chirp filter, where a processing gain of ∼17.3 dB, proportional to the time-bandwidth product of the filter, enables the recovery of a transmitted UWB signal in the presence of jamming.**

***Index Terms*—Chirp filter, finite impulse response filters, jamming, microwave photonics, optical frequency combs, optical processing, phase filter, programmable filters, pulse compression.**

I. Introduction

SPREAD spectrum radio-frequency (RF) pulse compression has been used in many applications, specifically sensing, ranging, communications, and imaging [1]–[3]. In these settings, achieving a high resolution is of great importance for precise measurement and range accuracy. In conventional ranging, short pulse widths, or equivalently large RF bandwidths, are desirable features for applications requiring high resolution. However, in these schemes, it is difficult to increase average transmitted power due to the consequent high peak power of the short pulses in peak power-limited RF transmitters, and as a result the ranging distance is limited [1]–[3]. Pulse compression solutions, on the other hand, not only allow the system designer to maintain high resolution, but also overcome the hurdle of peak power-limited transmitters and significantly extend the wireless operating distance.

Manuscript received March 25, 2015; revised August 18, 2015; accepted October 11, 2015. Date of publication November 17, 2015; date of current version December 02, 2015. This work was supported in part by the Office of the Assistant Secretary of Defense for Research and Engineering under the National Security Science and Engineering Faculty Fellowship program under Grant N00244-09-1-0068 from the Naval Postgraduate School, and by the Basic Science Research Program through the National Research Foundation of Korea (NRF) funded by the Ministry of Education (NRF-2014R1A6A3A03059647).

The authors are with the School of Electrical and Computer Engineering, Purdue University, West Lafayette, IN 47907-2035 USA (e-mail: sjun27@purdue.edu; arashidi@purdue.edu; amw@purdue.edu).

Color versions of one or more of the figures in this paper are available online at http://ieeexplore.ieee.org.

Digital Object Identifier 10.1109/TMTT.2015.2495172

In electronics, spread spectrum signal correlation—required at a receiver for pulse compression applications—can be performed by digital and analog methods. Digital signal processors can process arbitrary waveforms with a high degree of flexibility. The bandwidth of these processors depends on the sampling rate of analog-to-digital converters. Recently, analog-to-digital converters with several GHz bandwidths are commercially available and enable wideband digital signal processing [4], [5]. However, as the bandwidth increases, the effective number of bits decreases and a relatively long processing time is incurred in large time-bandwidth product (TBP) scenarios [5], [6]. Thus, digital signal processors are hard to apply for real-time ultrawideband (UWB) applications.

Unlike the digital methods, analog receiver technology can enable real-time UWB signal processing. For spread spectrum signal correlation there are two main analog methods: stretch processing and matched filtering. Stretch processing is applicable to the case of chirped waveforms. In this method the received waveform is mixed with a reference waveform, which is a replica of the transmitted waveform and which can be generated using tunable voltage-controlled oscillators [3], [7]. For a linear frequency chirp signal, the mixer output is a narrowband signal whose frequency depends on the relative time delay of the received and transmitted waveforms. Hence, stretch processing of wideband waveforms can be implemented using mostly narrowband components. Due to this advantage, stretch processors have been widely used in many wideband applications. However, this technique generally causes a signal-to-noise ratio (SNR) loss that depends on the time delay [7]. As a result, stretch processors cannot be utilized in long range applications such as radar search function. Matched filtering is another analog technique that utilizes a pulse compression filter matched to a specific transmitted waveform, and is proven to have maximal SNR performance. This process results in the concentration of received signal power into a short pulse. In other words, the peak SNR is enhanced by the pulse compression gain (also known as processing gain), whereas noise and other unmatched signals are passed through without enhancement. This feature is the key characteristic of the matched filter or pulse compression filter that allows its high resistance to jamming and interference [1]–[3].

Surface acoustic wave (SAW) filters have been widely used as chirped pulse compression filters [8]–[13]. The center frequency and RF bandwidth of SAW filters are typically below 2 GHz, although several works have reported narrowband filter response with constant group delay in the frequency range of up to 10 GHz [3], [8], [9]. However, in high frequency and wideband settings, SAW filters have two main limitations: lack

of programmability and high insertion loss. Since the performance of SAW devices depends on prefabricated physical structures, programmable/tunable SAW filter technology is still very immature [10]. Furthermore, as the RF center frequency is increased, the requirement of thinner electrodes to avoid large distortion effects from reflections increases the device parasitic resistive loss [11]. Also, the process of broadening the RF bandwidth (e.g. resistive matching) contributes directly to an increase in the insertion loss [11]. For example, in [12] the insertion loss for a SAW pulse compression filter with an RF bandwidth of ∼1 GHz at 3.63 GHz center frequency is 23 dB. In addition, as reported in [13], the insertion loss of SAW pulse compression filters is increased by 20–30 dB when the RF fractional bandwidth is increased from 25% to 50% at a center frequency of ∼5 GHz. Due to these performance limitations, it is very unattractive to employ SAW pulse compression filters in UWB settings.

Photonics-based schemes for spread spectrum pulse compression can provide wider RF bandwidths and thus achieve higher resolution along with versatile programmability. During the last several years, many different RF photonic schemes have been presented to implement UWB pulse compression filters [14]–[19]. For example, schemes using a continuous-wave laser utilize a hyperfine resolution pulse shaper [14] and fiber Bragg grating [15], respectively, to process an RF-modulated optical signal for pulse compression. The programmable scheme using the optical pulse shaper had an RF bandwidth of 15.5 GHz [14]. However, the time-aperture of the scheme (∼0.8 ns) was short, which was limited by the resolution of the shaper. By incorporating incoherent optical noise sources, schemes such as [16], [17] can provide larger time apertures, up to 15 ns with 5 GHz RF bandwidth at a center frequency of 32.5 GHz [17]. However, due to the poor noise performance of these methods, pulse compression was not successfully demonstrated. A noteworthy example of RF photonic pulse compression filtering is [18], where time-spectrum convolution enabled the use of multiple optical carriers in pulse compression of chirped microwave pulses with 3 GHz RF bandwidth and 3.8 ns time aperture in the presence of additive white noise. Further improvements of RF photonic schemes using multiple optical carriers show the potential for RF phase filtering via tapped delay line implementations based on a finite impulse response approach [19]–[24]. Among these schemes, those utilizing optical frequency comb sources provide simple scalability of the number of filter taps [19], [22]–[24]. In this area, recently our group demonstrated an optical frequency comb-based scheme with >160 comb lines, successfully demonstrating pulse compression over larger time apertures (up to 16 ns) and an RF bandwidth of 2.1 GHz [19].

Although these photonics-based schemes provide large RF bandwidths and programmability, they all lack from the point of view of high insertion loss due to losses of the passive optical components and the conversion efficiencies of optoelectronic devices such as modulators and photodetectors. In several previous works [22], [25]–[27], the RF performance of photonics-based schemes for amplitude filters has been investigated, and improvements have been reported. However, to our knowledge optimization of RF photonic phase filters for a low RF loss has not been considered.

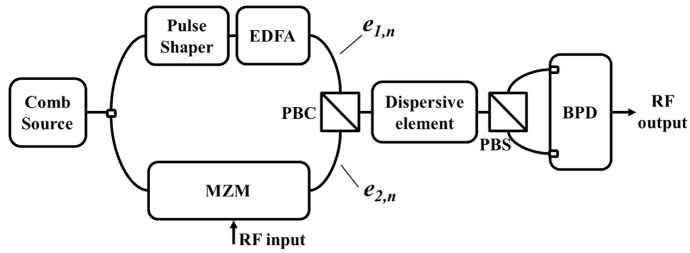

Fig. 1. Configuration of the RF photonic phase filter. (MZM: Mach-Zehnder modulator, PBC: polarization beam combiner, EDFA:erbium-doped fiber amplifier, PBS: polarization beam splitter, BPD: balanced photodetector).

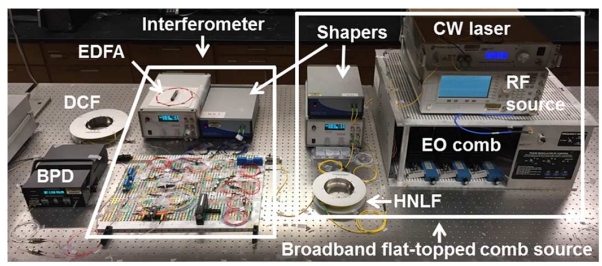

Fig. 2. Photograph of the RF photonic phase filter setup. (DCF: dispersion compensating fiber; HNLF: highly nonlinear fiber).

In this paper, a low-loss, ultra-broadband, and programmable RF photonic phase filter is demonstrated for pulse compression. In Section II, we describe our RF photonic phase filter and discuss the scaling of the output peak SNR enhancement. In Section III, we present the experiment and our results in detail. By increasing the output photocurrent and using an asymmetric input split ratio and balanced photodetection [22], the insertion loss of the filter is improved to only ∼0.5 dB after accounting for the internal matching resistor loss of the photodetector. We utilize this filter to demonstrate compression of linearly chirped waveforms with RF bandwidths up to 7.1 GHz and of binary phase-coded spread-spectrum signals. To further illustrate the generality of our programmable RF photonic phase filter, we successfully demonstrate pulse compression of a UWB Costas frequency-hopped spread spectrum signal with a 6 GHz RF bandwidth. Exploiting the low-loss and high processing gain capabilities of our setup, we demonstrate SNR enhancement by compressing a UWB chirp signal in the presence of jamming. Finally, we conclude in Section IV.

II. RF Photonic Phase Filter

Due to the fact that RF photonic phase filters using optical frequency combs are based on a finite impulse response approach, one can easily achieve features like versatile programmability and filter tunability. To have a high degree of programmability, a large number of filter taps is desirable. Comb-based schemes are advantageous since one can scale the number of filter taps. The schematic configuration and a photograph of the full RF photonic phase filter are shown in Figs. 1 and 2, respectively. The optical frequency comb is directed to an optical interferometer. One arm is sent to an erbium-doped fiber amplifier (EDFA) through a pulse shaper; while the other passes through a Mach-Zehnder modulator (MZM) biased at the minimum transmission point, in which optical carriers and optical noise are considerably reduced by the extinction ratio of the MZM [22], [28]. The outputs of

the EDFA and MZM are connected to a polarization beam combiner. The polarization-multiplexed signals are directed to a polarization beam splitter through a dispersive element. The use of a single dispersive fiber with polarization multiplexing allows us to match the two complementary signal paths for balanced detection [22]. The two outputs of the polarization beam splitter are then connected to the balanced photodetector (BPD).

Compared to our previous RF pulse compression experiment, that used a broadband Gaussian-shaped comb with a repetition rate of 10 GHz and an optical bandwidth of 12.8 nm [19], the current work makes several advances. First, the comb source has a larger comb spacing, wider comb bandwidth, and flat-topped shape. The larger comb spacing enables us to increase the filter bandwidth because the Nyquist zone (i.e., half of the comb spacing) is increased [23]. Also, the filter time aperture of comb-based schemes is given by the product of the comb's optical bandwidth and the dispersion. A flat-topped comb shape results in a larger time aperture than a Gaussian comb shape for the same number of comb lines and dispersion [17]. As a result, the TBP, the product of the filter's 3-dB RF bandwidth and time aperture, is greatly increased. Since the processing gain in pulse compression filters is limited by the TBP, the large filter TBP is desirable.

Second, we investigate—and substantially improve—the insertion loss of our RF photonic phase filter. Our achieved insertion loss is much lower than those of other photonic-based schemes as well as electronic SAW filters. To a large extent, the design of our phase filter follows the approach we introduced previously to improve the RF performance of a comb-based RF photonic amplitude filter [22]. By adopting an interferometer with asymmetric input split ratio, we optimize the path loss ratio related to the power difference between the optical carrier and sideband [22]. As a result the RF gain (i.e., the inverse of the RF loss) is maximized for a fixed photocurrent. Unlike the amplitude filter, however, the RF photonic phase filter places a programmable pulse shaper within one of the interferometer arms, so that not only the amplitude but also the phase of the mixing signals obtained at the output of the interferometer may be controlled.

Finally, to suppress the intensity noise originating from the optical amplification of the comb source needed to compensate the loss of the pulse shaper and other components and achieve high photocurrent, we also adopt two noise suppression techniques utilized in our previous work [22]: double-sideband modulation with suppressed carrier (DSB-SC) and balanced photodetection. The DSB-SC modulation corresponds to biasing the MZM at the minimum transmission point. As a result the MZM suppresses both the optical carriers and the intensity noise in the lower interferometer arm. Then the remaining common-mode intensity noise coming from the upper arm is substantially reduced by balanced detection. Balanced detection also has the advantage of increasing the RF gain by 6 dB [22]. These noise suppression techniques enable to produce compressed pulses with a high SNR, whereas previous photonic filtering schemes using incoherent optical sources suffer from high filter output noise [16], [17].

The quadratic phase related to the chromatic dispersion in the dispersive element can be expressed by [29]

$$\psi(\omega) = \psi_0 + \psi_1(\omega - \omega_0) + \frac{\psi_2}{2}(\omega - \omega_0)^2 \tag{1}$$

where ψ_2 is the coefficient for the second-order phase and ω_0 is the angular frequency of the optical carrier. The transfer function of the RF photonic phase filter is expressed by [19]

$$H(\omega_{RF}) \propto \sum_{n}^{N} a_n \exp\left(j\left[n\Delta\omega(\psi_2\omega_{RF} \pm \tau) \mp \varphi_n\right]\right) \tag{2}$$

where $a_n \sim e_{1,n}e_{2,n}$ is the RF amplitude of the nth tap, produced by beating the nth optical carrier (electric field amplitude $e_{1,n}$) and nth optical sideband (electric field amplitude $e_{2,n}$). $\Delta\omega$ is the comb spacing (i.e., optical pulse repetition rate); ω_{RF} is the angular RF frequency; τ is the delay difference between the two interferometer arms; and the φ_n represent the phases applied to nth optical comb line with the pulse shaper. Equation (2) indicates that our scheme is a finite impulse response filter [23]. The first phase term of (2) indicates linear group delay, introduced by the fiber dispersion, where $T(=\psi_2\Delta\omega)$ is the differential tap delay. In the absence of additional phase variation (φ_n), the summation results in bandpass RF filter response, with the passband frequencies shifted according to the delay difference τ [22]. In our DSB-SC modulation scheme, the different sidebands correspond to opposite signs of delay, pointed out by the $\pm\tau$ in (2). Hence there are two filter passband terms within one filter free spectral range $(\mathrm{FSR} = 1/T)$ [22]. Here we focus on one of the passbands for pulse compression within a single Nyquist zone.

In our current configuration, the amplitude of the nth optical carrier can be controlled by applying optical frequency dependent attenuation in the programmable pulse shaper. For bandpass filtering this provides the ability to programmably apodize the tap profile in order to vary the passband shape [23], [30]. In some applications amplitude windowing is also desired for pulse compression filters. For example, the Hamming window results in low time sidelobes and thus can mitigate intersymbol interference and false alarms in communication and ranging [3]. In our previous work on comb-based phase filtering [19], we chose a Gaussian windowing of the tap amplitudes, which yields a Gaussian passband shape for a linear chirp. In the current paper, the optical carrier power is controlled in the pulse shaper to provide a flat tap amplitude profile, which increases filter TBP.

Pulse compression action depends on the ability to control the phases of the taps. These may be programed by applying the desired optical phases (φ_n) in the pulse shaper; interference between carriers $e_{1,n}$ from the upper branch of the interferometer and sidebands $e_{2,n}$ from the lower branch of the interferometer transfers the optical phases into the electrical domain. For example, a quadratic RF phase response (or linear chirp delay response) can be achieved by applying a quadratic spectral phase function to the optical carriers $(\varphi_n = \beta n^2)$ [19]. Based on frequency-to-time mapping [23], [31], the spectral phase function

sampled by the comb of optical carriers is mapped into the temporal phase of the RF filter impulse response. Thus, after adequate dispersion, the temporal RF phase $\varphi_{RF}(t)$ can be expressed as

$$\varphi_{RF}(t) = \omega_C t + \frac{\beta}{T^2} t^2 \tag{3}$$

where ω_C $(= \tau/\psi_2)$ is the angular RF frequency at the center of the filter passband. Hence, the filter chirp rate is

$$\frac{\partial^2 \varphi_{RF}(t)}{2\pi \partial t^2} = \frac{\beta}{\pi T^2}. \tag{4}$$

In other words, the quadratic temporal RF phase response, achieved by the pulse shaping and frequency-to-time mapping, results in a frequency chirp (units GHz/ns or equivalent) that is linearly proportional to the β parameter and inversely proportional to the square of the tap delay T. Note that (4) corrects a factor of two error in the expression in our group's previous publication [19]. An important point is that the filter chirp rate can be tuned by the β parameter, which is related to the optical quadratic spectral phase programed by the pulse shaper. The programmable RF phase response of our scheme allows us to utilize it in matched filter settings, such as pulse compression. Assuming that the filter is programed to match the input RF signal and the noise generated inside the filter is negligible at the filter output, its performance can be quantified based on the output peak SNR to the input average SNR ratio as follows [32]

$$\frac{\mathrm{SNR}_{\mathrm{out,peak}}}{\mathrm{SNR}_{\mathrm{in,avg}}} = 2 \times \mathrm{TBP} \tag{5}$$

where $\mathrm{SNR}_{\mathrm{out,peak}}$ is the ratio of the output peak signal power to the output average noise power and $\mathrm{SNR}_{\mathrm{in,avg}}$ is the ratio of the input average signal power to the input average noise power. From (5), one can see that increasing the maximum achievable TBP of the filter allows higher output peak SNR to the input average SNR ratios. In our scheme the TBP depends on the number of optical comb lines [19].

Based on [33], in pulse compression, when the filter is perfectly matched to the input signal, the output peak signal power can be determined using the following equation:

$$\frac{\mathrm{P}_{\mathrm{out,peak}}}{\mathrm{P}_{\mathrm{in,peak}}} = \mathrm{TBP} \times G_{\mathrm{RF}} \tag{6}$$

where $\mathrm{P}_{\mathrm{in,peak}}$, $\mathrm{P}_{\mathrm{out,peak}}$, and G_{RF} are the input signal peak power, output compressed peak power, and the filter RF gain, respectively. The RF gain is equal to the inverse of the nominal RF loss $(\mathrm{L}_{\mathrm{RF}})$ of the filter. This nominal RF loss can be decomposed into $\mathrm{L}_{\mathrm{RF}} = \mathrm{L}_{\mathrm{E}} \times \mathrm{L}_{\mathrm{C}}$, where $\mathrm{L}_{\mathrm{E}} = \mathrm{TBP}$ is the expansion loss and L_{C} is the component loss or filter insertion loss [33], [34]. The expansion loss arises because manipulating the tap phases (the φ_n's) broadens the filter bandwidth while preserving the energy under the filter response. As a result, we have

$$\frac{\mathrm{P}_{\mathrm{out,peak}}}{\mathrm{P}_{\mathrm{in,peak}}} = \frac{1}{\mathrm{L}_C}. \tag{7}$$

Equation (7) clearly shows the importance of low component insertion loss in pulse compression filters. As mentioned in the introduction, high insertion loss is a great disadvantage for SAW-based pulse compression filters at high frequencies and wide bandwidths. The SAW-based pulse compression filter reported in [12] (1 GHz bandwidth at 3.6 GHz center frequency) had a 23 dB filter insertion loss, with reference to (7). In addition, the filter insertion loss would be significantly increased with the further increase of RF bandwidth [9]. However, as will be discussed in later sections, in our scheme, by incorporating optical amplifiers, asymmetric input split ratio of the interferometer, and balanced detection, we effectively bring the RF component insertion loss L_{C} down to nearly 0 dB, while increasing the RF bandwidth to >7 GHz. Furthermore, our photonic approach should be able to maintain similar performance even when scaled up to substantially higher RF frequencies and wider RF bandwidths.

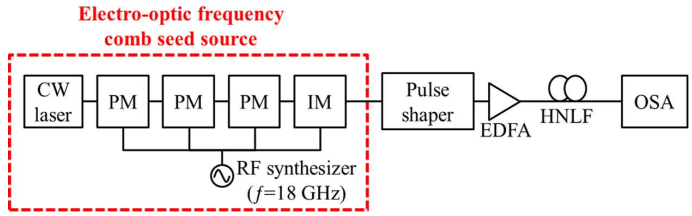

Fig. 3. Schematic diagram of the broadband and flat-topped comb source. (PM: phase modulator, IM: intensity modulator, EDFA: erbium-doped fiber amplifier, HNLF: highly nonlinear fiber, OSA: optical spectrum analyzer).

III. Experiment and Results

A. Broadband and Flat-Topped Comb Source

To achieve higher filter TBP values, a broadband and flat-topped optical comb source is required. Fig. 3 shows a schematic diagram of the generation setup for this source. In order to have a wider comb bandwidth, self-phase modulation-based spectral broadening in a highly nonlinear fiber (HNLF) is utilized [35]–[38]. In addition to the spectral broadening, a flat-topped comb shape can be achieved using seed pulses with appropriately shaped temporal profiles [36], [37]. Here, as the seed source, an electro-optic frequency comb source is used, having advantages such as tunable GHz repetition rate and good flatness [39], [40]. Due to these advantages, a spectrally broadened electro-optic frequency comb provides more flexibility for implementing the phase filters than a mode-locked laser [38]. In the electro-optic comb generation subsystem, a continuous-wave laser is connected to four cascaded electro-optic modulators including three phase modulators and one intensity modulator, where a single-frequency electrical RF signal generated by the RF synthesizer drives the four modulators [40]. In this experiment, the frequency of the electrical RF signal is set to 18 GHz, which directly determines the comb repetition rate. The seed comb is then directed to a programmable pulse shaper (Finisar WaveShaper 1000S), set to yield a parabolic pulse spectrum. We choose the parabolic pulse as the seed pulse shape to the HNLF, which results in a flat-topped shape after spectral broadening in the HNLF. In addition, it does not cause wave-breaking in the spectral broadening process and thus results in a very fast roll-off in the generated optical spectrum [37], [38]. The resultant pulse is amplified by the EDFA and directed to 150 meters of HNLF with dispersion of -1.88 ps/nm/km, nonlinear coefficient of 10 (W

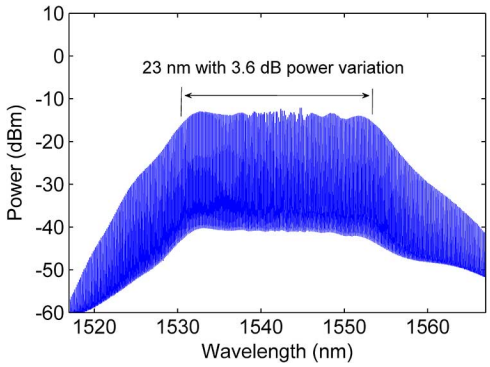

Fig. 4. Measured spectrum of the broadband flat-topped optical frequency comb (Resolution = 0.01 nm).

$\cdot\,\mathrm{km})^{-1}$, and fiber attenuation of 0.22 dB/km. Fig. 4 shows the optical spectrum of our broadened comb at the HNLF output. The broadened comb has ~23 nm optical bandwidth within a 3.6 dB power variation, containing 161 comb lines.

B. Linear Chirp Filter

In this section, linear chirp filters with different chirp rates are demonstrated to compress chirped RF pulses. In the programmable optical pulse shaper, located in the upper interferometer arm, 161 comb lines are appropriately shaped while the other comb lines are suppressed. In order to produce a constant RF beat power for all comb lines, the optical carrier powers are adjusted in the pulse shaper via amplitude shaping. We utilize a split ratio of 10:90 at the input to the interferometer (90% of the power directed to the MZM). The MZM in the lower interferometer arm has a half-wave voltage of 3 V at 1 GHz and an extinction ratio of 20 dB. As a dispersive element we use a spool of dispersion compensating fiber (DCF) with a dispersion of −400 ps/nm. The total output photocurrent is 17 mA. The maximum time aperture of the chirp filter is ~9.1 ns, and the filter FSR is 17.5 GHz because the differential delay between filter taps is ~57 ps. Also, the maximum RF bandwidth is 9 GHz, set by the width of the Nyquist zone which is equal to half of the 18 GHz optical comb spacing.

Fig. 5 shows the measured filter frequency responses of amplitude and group delay for various chirp rates, observed using a 0–20-GHz vector network analyzer. Due to the inevitable higher order dispersion in the DCF, dominated by cubic spectral phase, the filter phase response is slightly quadratic even when no phase is programed onto the pulse shaper. This initial RF quadratic phase is compensated by applying a calibration quadratic phase ($\beta = -0.0033$) in the pulse shaper. Then, the group delay becomes constant and the filter passband of the amplitude filter is a Sinc shape because of the flat amplitude coefficient. According to Fig. 5(a), the RF gain at the filter center frequency of 4.5 GHz is approximately −0.8 dB, with 100 MHz 3-dB RF bandwidth.

Then, we further increase the β parameter from 0.0008 to 0.0067 to tune the chirp rates. It is observed from Fig. 5 that as β is increased, the filter bandwidth increases while the RF gain comes down. This is a manifestation of the expansion loss mentioned earlier. The filter 3-dB bandwidths and average RF losses with β parameters of 0.0008, 0.0031, and 0.0067 are 2.63,

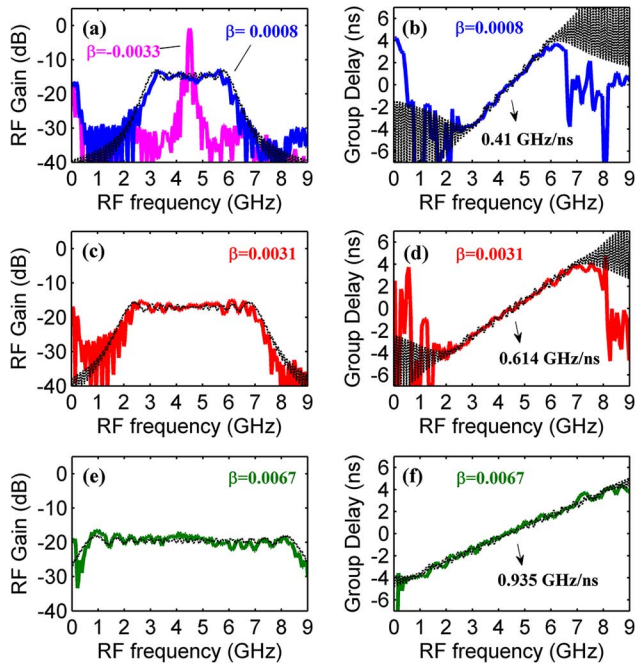

Fig. 5. Filter frequency responses for tuning of filter bandwidths and chirp rates. Amplitude responses with the β parameters of (a) −0.0033 and 0.0008, (c) 0.0031, and (e) 0.0067; Group delay responses with the β parameters of (b) 0.0008, (d) 0.0031, and (f) 0.0067; Colored solid and black dashed lines are measured and simulated data, respectively.

4.7, and 7.1 GHz, and 14.7, 16.8, and 19.2 dB, respectively. The chirp rates with the β parameters of 0.0008, 0.0031, and 0.0067 are 0.410, 0.614, and 0.935 GHz/ns, respectively. Since an equivalent β value of −0.0033 is required to counteract the third-order dispersion in the DCF, after subtracting this number from the experimental β values, the measured filter frequency responses agree with simulation results based on (2), shown as black dashed lines in Fig. 5. In addition, our chirp rates match what is derived in (4). The amplitude and group delay ripples observed in the amplitude and group delay responses of Fig. 5 are less than 4 dB and 0.5 ns, respectively. The ripples originate from the sudden discontinuities at the edges of the tap profile. The ripples can be reduced by applying tapered windowing or increasing the filter TBP (i.e., the number of comb lines) [41], [42].

Note that all measured RF powers are reduced by a factor of 4 due to the internal resistive matching circuitry of the BPD. However, the BPD output without the matching interface can be directly connected to another component. In this case, the BPD acts as a current source due to very large impedance originating from its depletion region's reactive capacitive [43]. Thus, some applications have used photodetectors without matching interfaces to retrieve the original generated power, although it causes slight power fluctuations and bandwidth restriction. In conventional analog-optic links, it is common to consider the intrinsic RF gain without the matching interface [43], [44]. Thus, the numbers shown in this paper for RF power used for evaluation of the RF gain and insertion loss refer to the values before this internal matching resistor. In other words, to account for the internal matching resistor, 6 dB is added to the power values measured at the BPD output.

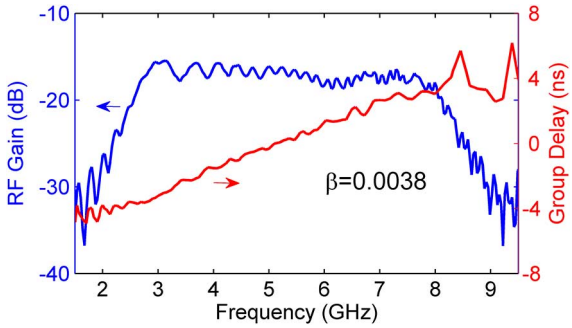

Fig. 6. Measured filter frequency response for pulse compression of binary phase-coded down-chirps.

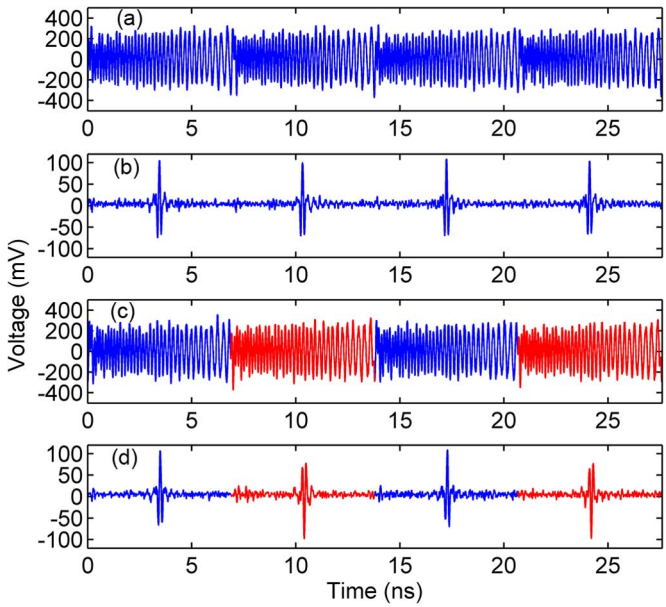

Fig. 7. Pulse comrpession of binary phase-coded down-chirps. (a) Measured input waveform and (b) measured output waveform with the sequence [1 1 1 1]. (c) Measured color-coded input waveform and (d) measured output waveform with the sequence [1 −1 1 −1].

C. Pulse Compression With Binary Phase Coding

Pulse compression can be combined with binary or higher-level phase coding to achieve various covert wireless communication schemes as well as high delay/Doppler resolution radar [1]–[3], [45]. Here we demonstrate pulse compression for a sequence of linear down-chirp pulses with data encoded onto successive down-chirp pulses via binary phase-shift keying (BPSK). The electrical input is generated by an electrical RF arbitrary waveform generator (Tektronix AWG7000C) programed to give down-chirp pulses with 0.725 GHz/ns chirp rate within a frequency range from 3 to 8 GHz. This corresponds to individual chirp waveforms with 6.9-ns time aperture and a TBP value of 34.5. The chirp waveforms repeat with 6.9 ns period, which is then BPSK modulated at ∼145 Mb/s. The chirp filter with a β parameter of 0.0038 is programed to have the opposite chirp rate of the down-chirp input pulses. Fig. 6 shows measured frequency response of the up-chirp filter. Fig. 7(a) and (c) show the measured input waveforms with BPSK sequences of [1 1 1 1] and [1 −1 1 −1], respectively, both having an average power of −2.3 dBm. Fig. 7(c) and (d) are color-coded based on the pulse polarity.

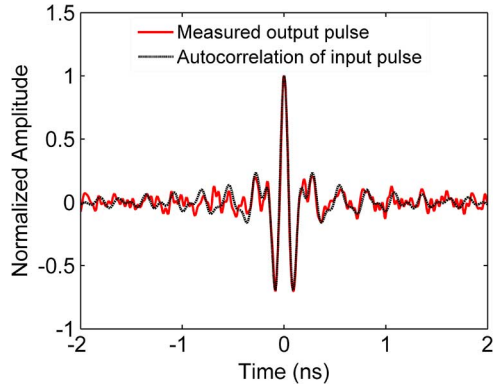

Fig. 8. Comparison of the measured output pulse and the autocorrelation of the measured input pulse.

As shown in Fig. 7(b) and (d), the measured peak voltages of the compressed pulses are approximately ±100 mV. After accounting for the internal matching resistor loss of 6 dB, the component loss (∼0.3 dB) is negligible because of the improved RF gain of the filter, resulting in a peak SNR of approximately 25 dB after pulse compression. As shown in Fig. 8, the measured output pulse shape agrees with its ideal form, which is the autocorrelation of the (measured) input pulse. This verifies that high fidelity pulse compression is achieved. These results indicate that the filter response is quite well matched to the input pulse waveform.

D. Frequency-Hopped Costas Sequence

Another very interesting set of waveforms with applications in synchronization and radar engineering are frequency-hopped spread-spectrum sequences. Among the various types of frequency-hopped sequences, Costas sequences are proven to have optimal compression characteristics, both in frequency (equivalent to Doppler resolution) and time (equivalent to range resolution) [2], [3]. To further illustrate the potential of our programmable RF photonic phase filter, we carry out experiments to compress a length-7 UWB Costas sequence with a fundamental frequency step of 0.86 GHz, centered at a 5 GHz carrier. The utilized Costas sequence harmonic ordering for the input signal to our phase filter in this experiment is $\{f_3, f_7, f_1, f_4, f_6, f_5, f_2\}$. Fig. 9(a) depicts the generated waveform using our electronic RF arbitrary waveform generator, having ∼6 GHz bandwidth and ∼8.2 ns time aperture. To further illustrate the frequency transitions, the normalized spectrogram of the pulse in Fig. 9(a) is calculated offline with a 0.7 ns Gaussian gate function and plotted in Fig. 9(b). For clarity, the corresponding instantaneous frequency harmonic of each section is also labeled on this plot.

To successfully compress the input pulse, the RF photonic phase filter must have a group delay response that is inversely matched to the response of the input pulse, i.e., the group delay values must follow the sequence $\{f_2, f_5, f_6, f_4, f_1, f_7, f_3\}$. Fig. 10(a) and (b) shows the measured amplitude and group delay responses of the programed Costas filter, respectively. From the comparison of Figs. 9(b) and 10(b), one can observe that the filter RF delay sequence is indeed inversely matched to that of the input Costas signal, as anticipated. In other words, the earlier the frequency component is received, the

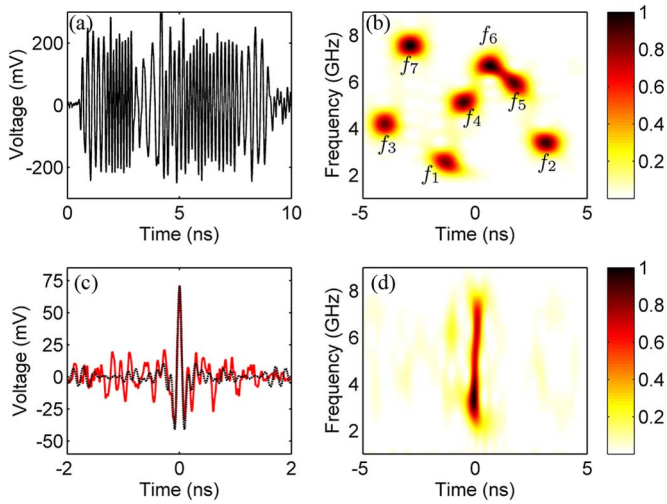

Fig. 9. Pulse compression with Costas sequence. (a) Waveform and (b) normalized spectrogram of the measured input pulse; (c) Waveform and (d) normalized spectrogram of the measured output pulse. In (c), the dashed line is autocorrelation of the measured input pulse.

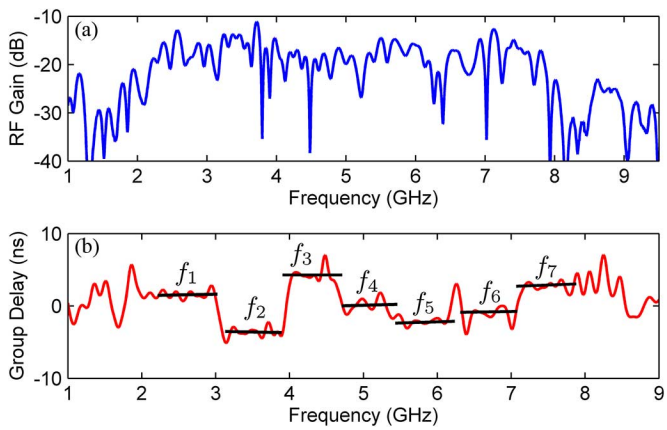

Fig. 10. Measured filter frequency responses for pulse compression with Costas sequence. (a) Amplitude response and (b) group delay response.

larger its group delay should be. As shown in Fig. 9(b), the filter receives frequency component f_3 earliest and frequency component f_2 latest. Therefore, the pulse compression filter imparts the largest group delay to the frequency component at f_3 and the shortest group delay to f_2. Fig. 9(c) shows the result of pulse compression overlaid with the autocorrelation of the input signal shown in Fig. 9(a). The normalized spectrogram of the measured pulse in Fig. 9(c) is calculated offline with a 0.3 ns Gaussian gate function and plotted in Fig. 9(d). As shown in Fig. 9(c), the compressed pulse is mostly matched to the autocorrelation. Although we have successfully achieved pulse compression, time sidelobes that are noticeably larger than those of the ideal compressed pulse are present. This is due to slight mismatch between the filter response and the input RF pulse, which is noticeable as slight group delay ripple in Fig. 10(b). The measured peak voltage is ~71 mV which gives a combined filter insertion loss and mismatch loss (due to nonideal compression) of approximately 3 dB, again after accounting for the internal matching resistor loss of 6 dB. As shown in Fig. 9(d), the spectrogram after passing through the

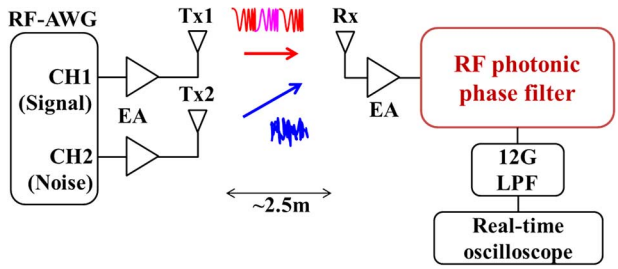

Fig. 11. Setup for the jamming-resistant pulse compression experiment. (Tx: transmitter; Rx: receiver; RF-AWG: RF-arbitrary waveform generator; EA: electrical amplifier; LPF: low-pass-filter).

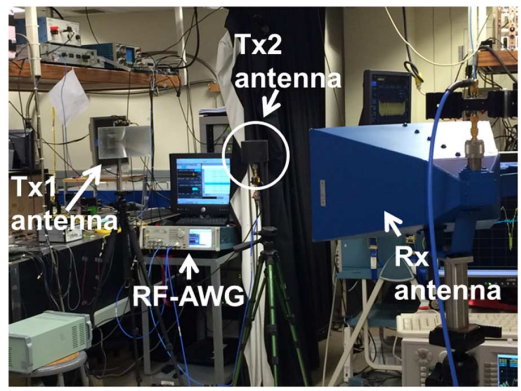

Fig. 12. Photograph of the jamming-resistant experimental setup.

RF photonic phase filter is nearly vertical, corresponding to a compressed pulse localized to a very short temporal duration (<150 ps).

E. Jamming-Resistant Pulse Compression

Jamming or interference is one of the important issues in modern radars and wireless communications [1], [2]. Pulse compression has resistance to jamming and interference because of the pulse compression or processing gain. In this section, we present pulse compression results on our RF photonic phase filter to show its jamming-resistant capabilities. The schematic setup and actual photograph for the jamming-resistant experiment are shown in Figs. 11 and 12, respectively. At the transmitter site, an electronic RF arbitrary waveform generator is used to transmit a linear down-chirp pulse as well as the UWB jamming noise. These signals are amplified and radiated by broadband antennas via an air channel to the receiver. At the receiver site, the detected down-chirp pulses, mixed with jamming noise, are amplified and directed to the phase filter with the β parameter of 0.0067. Fig. 13(a) and (b) show the waveform and normalized spectrogram (with a 0.7-ns Gaussian gate function) of the down-chirp pulse at the chirp filter input, when jamming noise is not present. As shown in Figs. 13(b) and 5(f), the down-chirp pulse and the phase filter have chirp rates of ± 0.935 GHz/ns over a 3-dB RF bandwidth of 7.1 GHz, respectively, thus a TBP of 54. Furthermore, the average power within the time aperture of the down-chirp pulse is -6.96 dBm (peak power $= -3.96$ dBm). The jamming noise has a flat spectrum with a 3-dB cutoff frequency of 8 GHz. The average power of the noise is -6.72 dBm. At the

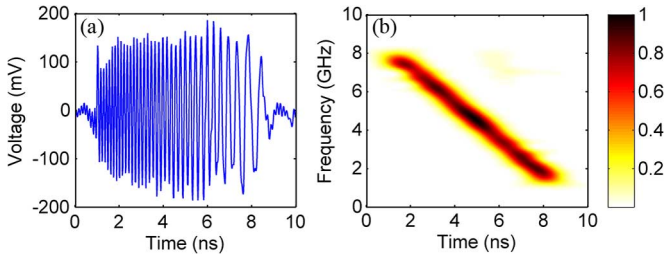

Fig. 13. (a) Waveform and (b) normalized spectrogram of the measured down-chirp pulse when jamming noise is not present.

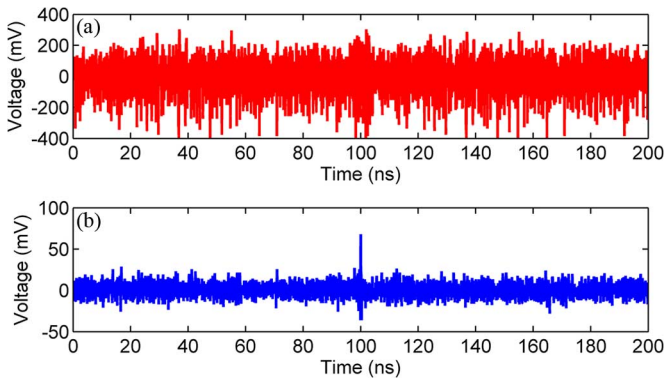

Fig. 14. Measured waveforms at (a) input and (b) output of the phase filter when jamming noise is present.

filter output, a low-pass-filter having a cut-off frequency of 12 GHz is used to suppress the comb beat note at 18 GHz.

Fig. 14(a) and (b) shows the measured input and output waveforms of the chirp filter, respectively, when jamming noise is turned on. At the input of the filter, as shown in Fig. 14(a), the down-chirp signal is not recognized at all among the high power jamming noise, making the input average SNR -0.24 dB. At the output, a compressed pulse with a peak voltage of 68 mV is clearly distinguishable from the noise floor. This leads to a peak power of -10.34 dBm, which is $\sim$6 dB lower than what is anticipated from (7), with filter insertion loss $\sim$0.38 dB. As mentioned before, this 6-dB difference is due to the fact that in our experiments, we did not compensate for the internal matching resistor loss of the BPD, as it would attenuate noise and signal in the same way hence not affecting the SNR.

From (5), an output peak SNR to the input average SNR ratio advantage of 108 $(2 \times \mathrm{TBP})$ would lead to the output peak SNR to be approximately $\sim$20.3 dB. In our experiments we measure an output peak SNR of 19.7 dB, which is very close to the ideal value. The slight discrepancy is caused by some excess noise introduced in the RF photonic phase filtering stage.

The TBP that can be handled in our scheme is proportional to the number of comb lines. In our current experiments using a comb with 3.6 dB optical bandwidth of 23 nm (161 comb lines), the TBP is $\sim$54. Recently, an ultra-broadband comb generation scheme was reported to yield a 10 GHz flat-topped comb with 1500 comb lines within 120 nm after spectral broadening [46]. By using such scheme to increase our number of comb lines, it should be possible to scale our RF photonic phase filtering approach for compression of UWB signals with TBPs in the range of several hundreds.

IV. Conclusion

We have demonstrated a low-loss, ultrawideband, and programmable RF photonic phase filter for pulse compression. It utilizes a broadband optical frequency comb, interferometric pulse shaping configuration, and balanced photodetection. Through experimental demonstrations, we show an UWB filter bandwidth of $>$7 GHz, well beyond what can be achieved in electronic SAW filters. The filter bandwidth can be extended using higher comb repetition rates. In addition, the insertion loss of our apparatus ($<$0.5 dB) is much lower than that of SAW filters ($>$23 dB) and other photonics-based schemes. We also have demonstrated high programmability with chirp rate tuning and Costas frequency-hopped sequence. Furthermore, we have demonstrated jamming-resistance with the UWB chirp filter. Although high power UWB jamming noise is transmitted to disturb the down-chirp signal, the compressed pulse is clearly recognized after pulse compression. Our data suggest that our scheme should be useful for many high resolution real-time RF pulse compression applications.

Acknowledgment

The authors would like to thank Mr. A. J. Metcalf, who developed the electro-optic frequency comb seed source utilized in these experiments, and Dr. D. E. Leaird, Dr. X. Xue, and Dr. M. Song for their technical assistance and valuable discussions. Any opinion, findings, and conclusions or recommendations expressed in this paper are those of the authors and do not necessarily reflect the views of the sponsors.

References

[1] A. W. Rihaczek, *Principles of High-Resolution Radar*. Norwood, MA, USA: Artech House, 1996.
[2] N. Levanon and E. Mozeson, *Radar Signals*. Hoboken, NJ, USA: Wiley-IEEE Press, 2004.
[3] M. I. Skolnik, *Radar Handbook*, 3rd ed. New York, NY, USA: McGraw-Hill, 1990.
[4] M. Moller, "High-speed electronic circuits for 100 Gb/s transport networks," presented at the OFC, San Diego, CA, USA, 2010, Paper OThC6.
[5] G. C. Valley, "Photonic analog-to-digital converters," *Opt. Exp.*, vol. 15, no. 5, pp. 1955–1982, 2007.
[6] S. M. Kuo, B. H. Lee, and W. Tian, *Real-Time Digital Signal Processing: Fundamentals, Implementations and Applications*. Hoboken, NJ, USA: Wiley, 2013.
[7] T. Long, Y. Wang, and T. Zeng, "Signal-to-noise ratio in stretch processing," *Electron. Lett.*, vol. 46, no. 10, pp. 720–722, 2010.
[8] H. Odagawa and K. Yamanouchi, "10 GHz range extremely low-loss ladder type surface acoustic wave filter," in *Proc. IEEE Ultrason. Symp.*, 1998, pp. 103–106.
[9] A. Hachigo, I. Nakahata, K. Itakura, S. Fujii, and S. Shikata, "10 GHz narrow band SAW filters using diamond," in *Proc. IEEE Ultrasonics Symp.*, 1999, pp. 325–328.
[10] K. Hashimoto, S. Tanaka, and M. Esashi, "Tunable RF SAW/BAW filters: Dream or reality?," in *Proc. IEEE Int. Freq. Control Symp. Eur. Freq. Time Forum*, 2011, pp. 1–8.
[11] R. M. Hays and C. S. Hartmann, "Surface-acoustic-wave devices for communications," *Proc. IEEE*, vol. PROC-64, no. 5, pp. 652–671, May 1976.
[12] R. Brocato, J. Skinner, G. Wouters, J. Wendt, E. Heller, and J. Blaich, "Ultra-wideband SAW correlator," *IEEE Trans. Ultrason., Ferroelectr., Freq. Control*, vol. 53, no. 9, pp. 1554–1556, Sep. 2006.
[13] R. Brocato *et al.*, "UWB communication using SAW correlators," in *Proc. IEEE Radio Wireless Conf.*, 2004, pp. 267–270.

[14] E. Hamidi and A. M. Weiner, "Phase-only matched filtering of ultrawideband arbitrary microwave waveforms via optical pulse shaping," *J. Lightw. Technol.*, vol. 26, no. 15, pp. 2355–2363, Aug. 2008.
[15] C. Wang and J. P. Yao, "Chirped microwave pulse compression using a photonic microwave filter with a nonlinear phase response," *IEEE Trans. Microw. Theory Techn.*, vol. 57, no. 2, pp. 496–504, Feb. 2009.
[16] X. Xue, X. Zheng, H. Zhang, and B. Zhou, "Tunable chirped microwave photonic filter employing a dispersive Mach-Zehnder structure," *Opt. Lett.*, vol. 36, no. 17, pp. 3518–3520, Sep. 2011.
[17] M. Bolea, J. Mora, B. Ortega, and J. Capmany, "Highly chirped single-bandpass microwave photonic filter with reconfiguration capabilities," *Opt. Exp.*, vol. 19, no. 5, pp. 4566–4576, 2011.
[18] M. Li, M. Antonio, L. Sophie, J. P. Yao, and J. Azana, "Reconfigurable and single-shot chirped microwave pulse compression using a time-spectrum convolution system," in *Proc. Microw. Photon. Int. Topical Meet. Microw. Photon. Conf.*, Oct. 2011, pp. 9–12.
[19] M. Song, V. Torres-Company, R. Wu, A. J. Metcalf, and A. M. Weiner, "Compression of ultra-long microwave pulses using programmable microwave photonic phase filtering with >100 complex-coefficient taps," *Optics Exp.*, vol. 22, no. 6, pp. 6329–6338, 2014.
[20] Y. Dai and J. P. Yao, "Nonuniformly-spaced photonic microwave delay-line filter," *Opt. Exp.*, vol. 16, no. 7, pp. 4713–4718, Mar. 2008.
[21] M. Sagues, A. Loayssa, and J. Capmany, "Multitap complex-coefficient incoherent microwave photonic filters based on stimulated Brillouin scattering," *IEEE Photon. Technol. Lett.*, vol. 19, no. 16, pp. 1194–1196, Aug. 2007.
[22] H.-J. Kim, D. E. Leaird, A. J. Metcalf, and A. M. Weiner, "Comb-based RF photonic filters based on interferometric configuration and balanced detection," *J. Lightw. Technol.*, vol. 32, no. 20, pp. 3478–3488, 2014.
[23] E. Hamidi, D. E. Leaird, and A. M. Weiner, "Tunable programmable microwave photonic filters based on an optical frequency comb," *IEEE Trans. Microw. Theory Techn.*, vol. 58, no. 11, pp. 3269–3278, Nov. 2010.
[24] V. R. Supradeepa, C. M. Long, R. Wu, F. Ferdous, E. Hamidi, D. E. Leaird, and A. M. Weiner, "Comb-based radio-frequency photonic filters with rapid tunability and high selectivity," *Nature Photon.*, vol. 6, pp. 186–194, 2012.
[25] I. Gasulla and J. Capmany, "Analytical model and figures of merit for filtered Microwave photonic links," *Opt. Exp.*, vol. 19, no. 20, pp. 19758–19774, Sep. 2011.
[26] K.-Y. Tu *et al.*, "Silicon RF-photonic filter and downconverter," *IEEE J. Lightw. Technol.*, vol. 28, no. 20, pp. 3019–3028, Oct. 2010.
[27] X. Xue, X. Zheng, H. Zhang, and B. Zhou, "Spectrum-sliced microwave photonic filter with an improved dynamic range based on a $LiNbO_3$ phase modulator and balanced detection," *IEEE Photon. Techn. Lett.*, vol. 24, no. 9, pp. 775–777, May 2012.
[28] C. Middleton and R. Desalvo, "High performance microwave photonic links using double sideband suppressed carrier modulation and balanced coherent heterodyne detection," in *Proc. IEEE Military Commun. Conf.*, 2009, pp. 1–6.
[29] A. M. Weiner, *Ultrafast Optics*, 1st ed. Hoboken, NJ, USA: Wiley, 2009, pp. 147–148.
[30] M. Song, C. M. Long, R. Wu, D. S. Seo, D. E. Leaird, and A. M. Weiner, "Reconfigurable and tunable flat-top microwave photonic filters utilizing optical frequency combs," *IEEE Photon. Technol. Lett.*, vol. 23, no. 21, pp. 1618–1620, Nov. 1, 2011.
[31] V. Torres-Company, D. E. Leaird, and A. M. Weiner, "Dispersion requirements in coherent frequency-to-time mapping," *Opt. Exp.*, vol. 19, no. 24, pp. 24718–4729, 2011.
[32] B. R. Mahafza, *Radar Systems Analysis and Design Using MATLAB*, 3rd ed. Boca Raton, FL, USA: CRC Press, 2013.
[33] C. Coo, *Radar Signals: An Introduction to Theory and Application*. New York, NY, USA: Academic Press, 1967.
[34] C. Campbell, *Surface Acoustic Wave Devices and Their Signal Processing Applications*. New York, NY, USA: Academic Press, 1989.
[35] R. Wu, V. Torres-Company, D. E. Leaird, and A. M. Weiner, "Supercontinuum-based 10-GHz flat-topped optical frequency comb generation," *Optics Exp.*, vol. 21, no. 5, pp. 6045–6052, 2013.
[36] C. Finot, B. Kibler, L. Provost, and S. Wabnitz, "Beneficial impact of wave-breaking for coherent continuum formation in normally dispersive nonlinear fibers," *J. Opt. Soc. Amer. B*, vol. 25, no. 11, pp. 1938–1948, 2008.
[37] F. Parmigiani *et al.*, "Ultra-flat SPM-broadened spectra in a highly nonlinear fiber using parabolic pulses formed in a fiber Bragg grating," *Opt. Exp.*, vol. 14, no. 17, pp. 7617–7622, 2006.
[38] A. Clarke, D. Williams, M. Roelens, and B. Eggleton, "Reconfigurable optical pulse generator employing a Fourier-domain programmable optical processor," *IEEE J. Lightw. Technol.*, vol. 28, no. 1, pp. 97–103, Jan. 1, 2010.
[39] R. Wu, V. R. Supradeepa, C. M. Long, D. E. Leaird, and A. M. Weiner, "Generation of very flat optical frequency combs from continuous-wave lasers using cascaded intensity and phase modulators driven by tailored radio frequency waveforms," *Opt. Lett.*, vol. 35, no. 19, pp. 3234–3236, Oct. 2010.
[40] A. J. Metcalf, V. Torres-Company, D. E. Leaird, and A. M. Weiner, "High-power broadly tunable electro-optic frequency comb generator," *IEEE J. Sel. Top. Quant. Electron.*, vol. 19, no. 6, Nov.–Dec. 2013, Art. ID 3500306.
[41] M. B. N. Butler, "Radar applications of S.A.W. dispersive filters," *IEE Proc.*, vol. 127, no. 2, pp. 118–124, 1980.
[42] M. Kowatsch and H. R. Stocker, "Effect of Fresnel ripples on sidelobe suppression in low time-bandwidth product linear FM pulse compression," *IEE Proc.*, vol. 129, no. 1, pp. 41–44, Feb. 1982.
[43] S. Iezekiel, *Microwave Photonics: Devices and Applications*. New York, NY, USA: Wiley–IEEE, 2009, pp. 150–152.
[44] C. Cox, *Analog Optical Links*. Cambridge, U.K.: Cambridge Univ. Press, 2004.
[45] G. F. Gott and J. P. Newsome, "H.F. data transmission using chirp signals," *Proc. IEE*, vol. 118, pp. 1161–1166, 1971.
[46] V. Ataie, E. Myslivets, B. P.-P. Kuo, N. Alic, and S. Radic, "Spectrally equalized frequency comb generation in multistage parametric mixer with nonlinear pulse shaping," *IEEE J. Lightw. Technol.*, vol. 32, no. 4, pp. 840–846, Feb. 15, 2014.

Hyoung-Jun Kim (S'06–M'10) received the B.S. degree in electrical engineering from Kwangwoon University, Seoul, Korea, in 2005, and the M.S. and Ph.D. degrees in electrical engineering from the Gwangju Institute of Science and Technology, Gwangju, Korea, in 2007 and 2011, respectively.

Since 2012, he has been working as a Postdoctoral Researcher in the Ultrafast Optics and Optical Fiber Communications Laboratory, Purdue University, West Lafayette, IN, USA. His research interests include microwave photonics, photonic signal processing, microwave and photonic integrated circuits, millimeter-wave radio access networks using radio-over-fiber, and optical frequency comb generation.

Dr. Kim serves as a Reviewer for *Optics Express*, IEEE PHOTONICS TECHNOLOGY LETTERS, and IEEE PHOTONICS JOURNAL. He received the Best Student Paper Award in Global Symposium on Millimeter Waves (2008), Excellent Research Award (2011) for his Ph.D. dissertation, and Korean government fellowships for National Research Graduate (2009) and Postdoctoral Fellow (2014).

Amir Rashidinejad (S'10–M'11) received the B.Sc. degree in electrical engineering from the Sharif University of Technology, Tehran, Iran, in 2011. He is currently working toward the Ph.D. degree at the Ultrafast Optics and Optical Fiber Communications Laboratory, Purdue University, West Lafayette, IN, USA, and the Ph.D. degree at the School of Electrical and Computer Engineering, Purdue University.

From 2009 to 2011, he was an undergraduate Research Assistant with the Advanced Communications Research Institute (ACRI) and the Optical Networks Research Laboratory (ONRL) at Sharif University. He is currently a graduate Research Assistant with the Ultrafast Optics and Optical Fiber Communications Laboratory, Purdue University. His research interests include radio-frequency photonics; optical pulse shaping; ultrabroadband microwave and millimeter-wave arbitrary waveform generation and processing; and applications in ranging and communication systems.

Andrew M. Weiner (S'84–M'84–SM'91–F'95) received the Sc.D. in electrical engineering from the Massachusetts Institute of Technology, Cambridge, MA, USA, in 1984.

Upon graduation, he joined Bellcore, first as a Member of Technical Staff and later as Manager of Ultrafast Optics and Optical Signal Processing Research. He moved to Purdue University, West Lafayette, IN, USA, in 1992, and is currently the Scifres Family Distinguished Professor of Electrical and Computer Engineering and has since graduated over 30 Ph.D. students. He has also spent sabbaticals at the Max Born Institute for Nonlinear Optics and Ultrashort Pulse Spectroscopy, Berlin, Germany, and at JILA, University of Colorado and National Institute of Standards and Technology, Boulder, CO, USA. He currently serves as Editor-in-Chief of *Optics Express*, an all-electronic, open access journal publishing more than 3000 papers a year emphasizing innovations in all aspects of optics and photonics. He is author of a textbook entitled "Ultrafast Optics" (Wiley, 2009), has published eight book chapters, over 300 journal articles, and over 500 conference papers, and invented 16 U.S. patents. He is especially well known for his pioneering work on programmable generation of arbitrary ultrashort pulse waveforms, which has found application both in fiber optic networks and in ultrafast optical science laboratories around the world. His research focuses on ultrafast optics, with a focus on processing of extremely high speed lightwave signals and ultrabroadband radio-frequency signals.

In 2008, Prof. Weiner was elected to membership in the National Academy of Engineering, and in 2009, was named a Department of Defense National Security Science and Engineering Faculty Fellow. He was the recipient of many awards, including the Hertz Foundation Doctoral Thesis Prize (1984), the Optical Society of America's Adolph Lomb Medal (1990) and R.W. Wood Prize (2008), the International Commission on Optics Prize (1997), the IEEE Photonics Society's William Streifer Scientific Achievement Award (1999), and Quantum Electronics Prize (2011). He was also the recipient of the inaugural Research Excellence Award from the Schools of Engineering (2003), the Provost's Outstanding Graduate Student Mentor Award (2008), the Herbert Newby McCoy Award for outstanding contributions to the natural sciences (2013), and the College of Engineering Mentoring Award (2014), all from Purdue University.